Fuzzy CT Metrology: Dimensional Measurements on Uncertain Data

Artem Amirkhanov *
Upper Austrian University of Applied Sciences
Christoph Heinzl †
Upper Austrian University of Applied Sciences
Christoph Kuhn ‡
Carl Zeiss
Johann Kastner §
Upper Austrian University of Applied Sciences
Meister Eduard Gröller ¶
Vienna University of Technology

Abstract

Metrology through geometric dimensioning and tolerancing is an important instrument applied for industrial manufacturing and quality control. Typically tactile or optical coordinate measurement machines (CMMs) are used to perform dimensional measurements. In recent years industrial 3D X-ray computed tomography (3DXCT) has been increasingly applied for metrology due to the development of XCT systems with higher accuracy and their ability to capture both internal and external structures of a specimen within one scan. Using 3DXCT the location of the specimen surface is estimated based on the scanned attenuation coefficients. As opposed to tactile or optical measurement techniques, the surface is not explicit and implies a certain positional uncertainty depending on artifacts and noise in the scan data and the used surface extraction algorithm. Moreover, conventional XCT measurement software does not consider uncertainty in the data. In this work we present techniques which account for uncertainty arising in the XCT metrology data flow. Our technique provides the domain experts with uncertainty visualizations, which extend the XCT metrology workflow on different levels. The developed techniques are integrated into a tool utilizing linked views, smart 3D tolerance tagging and plotting functionalities. The presented system is capable of visualizing the uncertainty of measurements on various levels-of-detail. Commonly known geometric tolerance indications are provided as smart tolerance tags. Finally, we incorporate the uncertainty of the data as a context in commonly used measurement plots. The proposed techniques provide an augmented insight into the reliability of geometric tolerances while maintaining the daily workflow of domain specialists, giving the user additional information on the nature of areas with high uncertainty. The presented techniques are evaluated based on domain experts feedback in collaboration with our company partners.

CR Categories: Computer Graphics [I.3.8]: Applications

Keywords: industrial 3D computed tomography, uncertainty visualization, level-of-details, metrology

*e-mail: artem@cg.tuwien.ac.at
†e-mail: Christoph.Heinzl@fh-wels.at
‡e-mail: c.kuhn@zeiss.de
§e-mail: Johann.Kastner@fh-wels.at
¶e-mail: groeller@cg.tuwien.ac.at

1 Introduction

Geometric tolerancing and dimensional measurements are well established methods in industrial quality control. They are the basis of assuring the manufacturing quality of industrial products. In most cases tactile measurements using coordinate measurement machines (CMMs) or optical coordinate measurement techniques are the methods of choice.

An emerging technology in the field of dimensional measurement is three-dimensional X-ray computed tomography (3DXCT). 3DXCT is a powerful technique for generating a 3D volumetric dataset of a specimen from 2D X-ray penetration images (projections). The set of 2D projections is acquired by irradiating the scanned object with X-rays. A reconstruction algorithm is then applied to the projections to compute the corresponding 3D dataset of the scanned specimen. The ability to measure structures which are not accessible by CMMs as well not-metrology-friendly materials (e.g., transparent, reflecting, soft, or deformable specimens) makes 3DXCT a very attractive tool for metrology purposes. However, one important distinction of 3DXCT from conventional CMMs is that the surface of the object is not explicitly defined. Tactile or optical measurements probe the actual surface of a specimen. In contrast, only a 3D volume of attenuation coefficients is available. The material interfaces detection is one of the most critical aspects regarding dimensional metrology using 3DXCT. The quality of the material interfaces may spatially vary considerably due to various artifacts and irregularities, which are present in the 3DXCT volume data. In every stage of the 3DXCT metrology workflow there are several parameters and influencing factors which affect and propagate errors and uncertainty. Firstly, during the *scanning stage* the resulting quality of the scan is affected by several groups of factors, e.g., by scanning parameters, various physical phenomena, or scanning artifacts like noise, ring artifacts, or scattered radiation. Secondly, when the *3D reconstruction* is performed, artifacts may also be introduced by the used 3D reconstruction algorithm, e.g., metal artifacts and streaking artifacts.

Currently the estimated surface location is considered as the ground truth and the uncertainty of this surface is not taken into account during the measurement analysis and evaluation. In this work we propose a technique which accounts for positional uncertainty in industrial 3DXCT metrology. The general workflow is shown in Figure 1. The presented 3DXCT metrology system accounts for measurement uncertainty by incorporating two stages: the preprocessing stage and the uncertainty visualization stage. The preprocessing stage consists of two steps: probing of the measurement

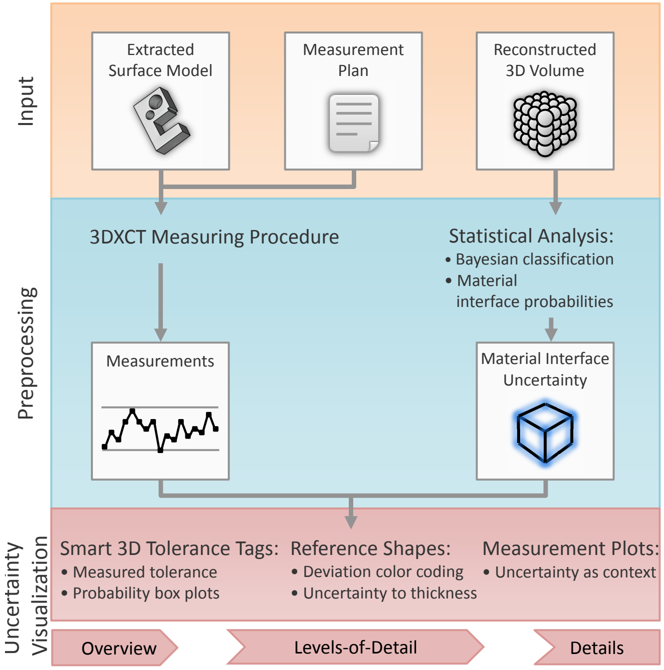

Figure 1: Workflow of 3DXCT dimensional metrology accounting for measurement uncertainty.

features and statistical analysis. Measurements meter the deviations of the evaluated features from ideal shapes such as lines, planes, circles, or cylinders (section 3). The 3D surface model extracted from the reconstructed 3D volume is then used to perform measurements. During the 3DXCT measuring a list of such measurements from a measurement plan is evaluated. The data of the measurements are then further propagated in the workflow to the uncertainty visualization stage. As a second preprocessing step, we use statistical analysis (section 4) on the reconstructed 3D volume to estimate the uncertainty of the material interfaces of the specimen. Then, during the uncertainty visualization stage (section 7), we encode information about uncertainties in graphical representations commonly used for measurement analysis and for evaluation by metrology experts. The design of our uncertainty visualizations follows Shneiderman's visual information seeking mantra [Shneiderman 1996]: "Overview first, zoom and filter, then details-on-demand". The uncertainty of measurements is depicted on various levels-of-detail. First, an overview of the measurement uncertainties is provided using smart 3D tolerance tags (section 5) and reference shapes (section 6). Then, we provide the detailed uncertainty information by enhancing measurement plots by visualizing the uncertainty context.

In their daily workflow domain specialists are only considering 2D representations in their workflow, and 3D is typically used to show the spatial position of the measurement features. Our approach does not modify the existing workflow of the domain experts for the evaluation of measurements. Our approach extends the common workflow with additional information about the underlying uncertainty of the measured data in order to improve the process of decision making and measurement evaluation. Additionally meaningful 3D visualisations are presented and several methods are used to support a visual linking with 2D measurement plots.

The main contributions of this paper are:

- a statistical analysis on the reconstructed 3D volume in order to estimate material interface probabilities
- the design of novel uncertainty visualization techniques providing information about measurement uncertainty on various levels-of-detail. The visualizations proposed are: encoding uncertainty using radii of the reference shapes, smart expandable 3D tolerance tags with probability box plots, and an extension of common measurement plots with uncertainty information as the context
- to present linked interactive views (Figure 2) using sliding pointers and smart 3D tolerance tag picking for supporting the exploration and visualization of the measurements' uncertainty.

2 Related Work

Geometric tolerancing and metrology for quality control is defined in various standards: the ISO standards and American Standard ASME Y14.5M. Geometric tolerances are usually communicated using a symbolic language on engineering drawings. The description of the current state of the art regarding geometrical dimensioning and tolerancing can be found in the literature, e.g., in the book of Georg Henzold [Henzold 2006]. As the geometric tolerancing techniques themselves are considered as being out of the scope of this work they are not addressed any further.

The origin of uncertainty in 3DXCT scans is influenced by many factors. First, there is a large parameter space for calibrating the 3DXCT device itself [Kruth et al. 2011]. These parameters have to be specified by a system technician before the scanning procedure: the X-ray source defines the characteristics of the emitted X-rays regarding intensity and quality of the beam [Ball and Moore 1997]. This is the first major origin of uncertainty in 3DXCT scan. The geometry of the specimen as well as its position and orientation in the X-ray beam may further influence the quality of an X-ray scan [Amirkhanov et al. 2010]. Additionally, various physical phenomena occurring during the 3DXCT scanning can affect the final result. One example of such phenomena are temperature drifts of the 3DXCT system's components (X-ray source, motors, drives, detector, electronics), as well as temperature changes in the specimen. These drifts and changes may be corrected using temperature compensation techniques [Kruth et al. 2001]. Finally, 3DXCT scans may contain various artifact types. Artifacts are defined as artificial structures in the dataset which do not correspond to reality [Heinzl 2009]. The most prominent example is beam hardening which denotes the effect of low energy X-ray photons being attenuated stronger than high energy photons. This results in contrast deterioration and nonlinearities in the reconstructed 3D volume. The beam hardening effects may be overcome using linearization techniques [Kasperl et al. 2002].

Uncertainty visualization is considered as one of the top visualization research challenges [Johnson 2004]. An overview of applications for uncertainty visualization is given in the survey by Zuk and Carpendale [Zuk and Carpendale 2006]. An early work of Rheigans and Joshi [Rheingans and Joshi 1999] is dealing with visualization of molecules with positional uncertainty. Various visualizations depicting the uncertainty of isosurfaces are explored by Rhodes et al. [Rhodes et al. 2003]. In the work by Berger et al. [Berger et al. 2011] uncertainty is visualized with regards to a potentially insufficient sampling density and inaccurate predictions for multidimensional parameter spaces. Coninx et al. [Coninx et al. 2011] visualize areas with high uncertainty by adding animated Perlin noise. Various uncertainty visualization possibilities combined with

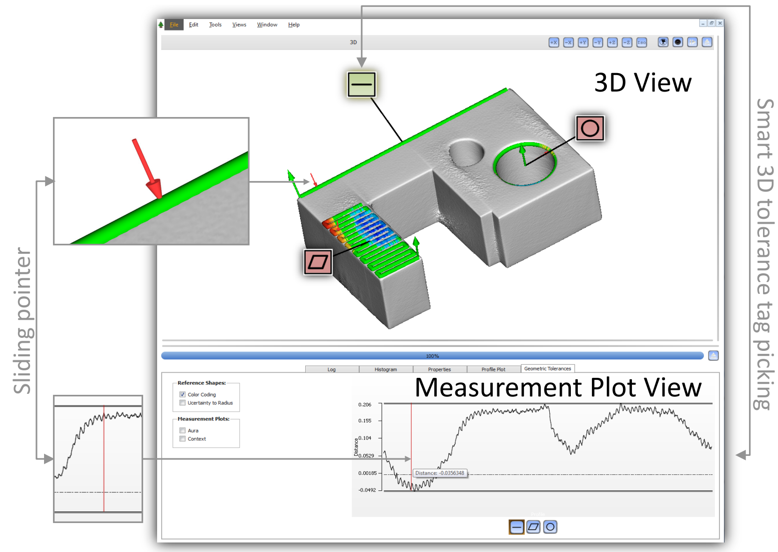

Figure 2: The application's user interface. Visual linking methods are indicated.

volume rendering are explored by Djurcilov et al. [Djurcilov et al. 2002]. Grigoryan and Rheingans [Grigoryan and Rheingans 2004] use a point cloud approach to depict spatial uncertainty in the data. Combined probabilistic classification results from multiple segmentations are visualized to allow risk estimation in the work by Kniss et al. [Kniss et al. 2005]. Saad et al. [Saad et al. 2010] introduce an interactive analysis and visualization tool for probabilistic segmentation in medical imaging utilizing appearance prior information extracted from expert-segmented images. Prassni et al. [Prassni et al. 2010] have presented a user assisted segmentation tool improving the segmentation in an iterative feedback loop by minimizing segmentation uncertainty. Partial range histograms are introduced in the work by Lundström et al. [Lundström et al. 2006] to enable an automatic statistical classification. In another paper Lundström et al. [Lundström et al. 2007] explore uncertainty visualization in medical volume rendering using probabilistic animations for medical diagnosis. An application of uncertainty visualization in a flooding simulation scenario is given by Waser et al. [Waser et al. 2011]. The presented system accounts for input uncertainties and explores how these uncertainties in the boundary conditions affect the confidence of a simulation. Pauly et al. [Pauly et al. 2004] construct likelihood and confidence maps for a surface from a set of sampled points. Applications include adaptive re-sampling, an algorithm for reconstructing surfaces in the presence of noise, and robust merging of a set of scans into a single point-based representation. Pöthkow et al. [Pöthkow and Hege 2010] explore in their work the positional uncertainty of iso-contours. The presented visualizations are combining color coded isosurfaces with the uncertainty information depicted using direct volume rendering. In the following year two interesting papers have elaborated on the positional uncertainty of isosurfaces: Pöthkow et al. [Pöthkow et al. 2011] introduced a probabilistic marching cubes method taking into account statistical correlations between probabilities. Pfaffelmoser et al. [Pfaffelmoser et al. 2011] consider correlations between random functions and introduce an incremental update scheme that allows to integrate the probability computation into front-to-back volume ray-casting. The statistical analysis method in this work is partially inspired by the ideas presented in the last two papers. Mapping the uncertainty to visual properties as employed in many of the above mentioned papers motivated our uncertainty to radius mapping for the reference shapes.

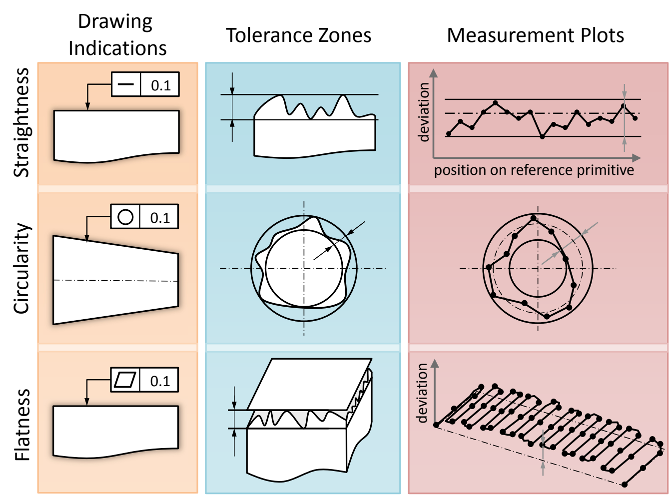

Figure 3: Straightness, circularity, and flatness geometric tolerances.

3 Geometric Tolerancing

Industrial workpieces should usually be manufactured as precisely as possible. However, in practice it is impossible to produce them without deviations to the desired reference shapes. This obliges manufacturers to adhere to required tolerances for the assembly or other subsequent processes. Thus, the workpiece is reduced to a set of features or geometrical elements, such as edges, planes, cylinders, cones, spheres, etc.. Geometrical tolerances are specified for these features in order to keep the deviations within acceptable ranges. Measurements are performed, compared with the given tolerances, and further evaluated. Evaluations using visual representations like measurement plots are carried out in cases which are particularly interesting for the experts. Following the corresponding ISO Standard there exists a fixed set of geometric tolerances [Henzold 2006] which concern deviations of features from the ideal shapes. These shapes are called *reference shapes*. They include line profiles, circles, planes, cylinders, etc. Reference shapes are specified explicitly in the measurement plan. The type, positioning, orientation as well as size of the reference shapes are given.

In this paper we focus on three types of geometric tolerances [Henzold 2006]: straightness, circularity, and flatness (see Figure 3). However, the presented approaches are expandable to any other dimensional measurement features. *Straightness* is a geometric tolerance which specifies how much the measured feature may deviate from an ideal straight line. The straightness of a feature is measured by sampling a set of points on the specimen surface while a probing tool is moving along an ideal straight line. The measured profile shall be contained between two parallel lines denoting the allowed tolerance. The measured data can be explored using a straightness plot (Figure 3 top/right). *Circularity* is a geometric tolerance that checks how much a feature may deviate from a perfect circle. It is measured by sampling a set of points on the specimen surface while a probing tool is moving along the ideal circle. The resulting profile (circumference) shall be contained between two coplanar concentric circles with a radial distance equal to the tolerance value. The measured data can be explored using a circularity plot (Figure 3 middle/right). *Flatness* is a geometric tolerance that evaluates how much a feature can deviate from an ideal plane. It is measured by sampling a set of points on the specimen surface while a probing tool is moving along a specific curve within the ideal plane. All points of the measured profile should be contained in a zone between two parallel planes of a fixed distance apart. Arbitrary or plane-filling curves are commonly used for probing. The measured data can be explored using a straightness plot as well.

The 3DXCT measuring procedure simulates a CMM probing process: A stylus is moving along the defined measurement trajectory on the specimen surface. The deviations from the reference shape are calculated for the probed points. In the case of 3DXCT the surface extracted from the reconstructed 3D volume is used to perform measurements. Ray casting is applied to determine the positions of the probed points on this surface. The investigated trajectory is uniformly sampled along the probing direction. A ray is cast from every point on the reference shape in the probing direction. To find a corresponding probed point an intersection of the ray with the surface is then calculated. The deviation at the probed point is the distance between the reference shape and the intersection point. Since the 3DXCT measuring procedure can operate on any provided surface, it is not restricted to a particular surface extraction algorithm. The surface generated by any advanced surface extraction method may be provided as input for measurements.

4 Statistical Analysis

We perform a statistical analysis on the 3DXCT data to introduce information on uncertainty, which characterizes the materials present in the data as well as information or the uncertainty of the corresponding material interfaces. We compute material interface probabilities for every voxel in two steps: First, we apply an automatic statistical classification based on Bayes' decision theorem (section 4.1). This classification uses the reconstructed 3D volume as input data. The classification calculates posterior probabilities for the attenuation coefficients in each voxel of the dataset of belonging to each of the materials present in the data. Second, we calculate material interface probabilities (section 4.2). This step takes the posterior probabilities as input and computes the material interface probability for every voxel of the volume. These probabilities are then stored in a material-interface probability-volume.

4.1 Bayesian Classification

The task of the Bayesian classification is to determine for every attenuation coefficient to which extent it belongs to the materials present in the dataset. We assume C different material classes $\omega_1, \omega_2, ..., \omega_C$. For example for a component made of plastic and metal: $\omega_1 \leftarrow$ air, $\omega_2 \leftarrow$ plastic, and $\omega_3 \leftarrow$ metal. Consider the attenuation value x. Lets denote $P(\omega_i|x)$ as the probability which indicates that x belongs to the corresponding material class ω_i, $i = 1, ..., C$. The classification assigns a vector of posterior probabilities $[P(\omega_1|x), P(\omega_2|x), ..., P(\omega_C|x)]$ to every attenuation value x. In this work we use an automatic Bayesian classification algorithm as described in the work by Heinzl et al. [Heinzl et al. 2008]. The classification is based on Bayes' decision theorem and consists of three major steps: feature selection, classifier selection, and estimation of the class conditional probability density function (PDF). In the first step, after a class is assigned to every material, the attenuation coefficients of voxels are used to specify the feature vector. In the second step, a reliable material classifier is chosen. Several assumptions are made for the 3DXCT data. First, homogeneous materials tend to generate constant attenuation coefficients. Second, due to various artifacts and irregularities introduced by the detector/X-ray source combination, the attenuation coefficients are modified on the borders of a material. Third, the normal (or Gaussian) distribution is often chosen in many applications to model such modifications. Consequently, a Gaussian distribution is assumed for the attenuation coefficients of each single material in the CT scan. During the last step, a custom automatic Gaussian curve fitting scheme is used to set up the PDF for every material (for details see [Heinzl et al. 2008]). Then the probability vector is calculated using Bayes' theorem. It weights the class conditional PDF against the observed evidence and the prior information. The prior information is set to $1/C$ for every ω_i, $i = 1, ..., C$. The evidence is defined as the sum of all class conditional PDFs. After the weighting the posterior probabilities $P(\omega_1|x), P(\omega_2|x), ..., P(\omega_C|x)$ are guaranteed to sum up to 1.

4.2 Material Interface Probabilities

We introduce material interface probabilities to represent the uncertainty of material transitions in the specimen. The surface will be a material interface when it segregates points belonging to one material from points of another material. Therefore, we assume that the face between two voxels belongs to a material interface when the neighbouring voxels belong to different materials. To illustrate this, consider two adjacent voxels A and B with corresponding attenuation values x_A and x_B. Lets denote a face between these voxels as $face_{A,B}$. Then the probability that the interface between any two materials is passing through this face can be calculated as follows:

$$P(face_{A,B} \text{ is interface}) = \sum_{i=1}^{C} \sum_{j=1, j\neq i}^{C} P((\omega_i|x_A) \cap (\omega_j|x_B)), \quad (1)$$

where $P((\omega_i|x_A) \cap (\omega_j|x_B))$ is the conditional probability that voxels A and B belong to different materials ω_i and ω_j for $i \neq j$. The computation of conditional probabilities requires the knowledge of correlations between the probabilities defined by the corresponding PDFs. Furthermore, the estimation of such correlations requires multiple realizations of the random variables. This could be achieved using multiple scans which is not affordable in the 3DXCT metrology scenario. Additionally, in many cases physical effects which increase correlations (e.g., radiation scattering or partial-volume artifacts) are rather weak and can be neglected. Based on these considerations, we assume that random variables

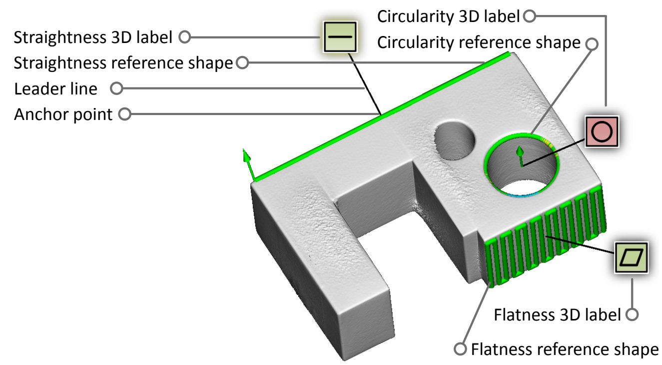

Figure 4: Smart 3D tolerance tags and reference shapes for: straightness of the specimen's edge, circularity of the specimen's drill hole, and flatness of the specimen's face.

defined by posterior material probabilities are *stochastically mutually independent*. This means that if any particular voxel is known to belong to a certain material, it is neither more nor less likely that any other voxel belongs to this or some other material. It is known that two random events E_1 and E_2 are stochastically independent if and only if the probability $P(E_1 \cap E_2) = P(E_1) * P(E_2)$. When taking this into account Eq. (1) will transform into:

$$P(face_{A,B} \text{ is interface}) = \sum_{i=1}^{C} \sum_{j=1, j\neq i}^{C} P(\omega_i | x_A) * P(\omega_j | x_B). \quad (2)$$

With Eq. (2) we can now compute the probability of a material interface for any face between two voxels. However, assigning the interface probability to faces results in a higher memory consumption. Therefore, we sample this representation into the conventional 3D volume having to store just one value for each voxel. For each voxel we average the material interface probabilities of all its faces. The obtained probabilities are no longer represented by the PDFs since probabilities are not assigned to the attenuation coefficients but to the individual voxels. Every voxel can be considered as a separate random event which has two possible outcomes: the voxel contains an interface between two different materials or the voxel does not contain any interface. The probabilities of these two events sum up to 1 for every voxel. The interface probabilities of voxels are stored in the interface probability volume. After the statistical analysis we have an interface probability volume which estimates interface probabilities instead of a conventional surface estimation (e.g., isosurface).

The presented method for estimating material interface probabilities provides a strong response at the boundaries of different materials. It results in sharp material edges and it is robust with respect to noise and low contrast. The algorithm is highly parallel and it is well suited for a fast GPU-based implementation. However, computing a 3D interface probability volume consumes additional memory.

5 Smart 3D Tolerance Tags

Tolerance indications using tags are commonly employed in dimensional metrology for indicating geometric tolerances on 2D drawings (as seen in Figure 3). The indication usually consists of the following elements: an arrow pointing at the toleranced feature, a symbol indicating tolerance type and allowed tolerance value. Based on this notion we introduce *smart 3D tolerance tags*. The tags are drawn on the canvas of the 3D view and indicate measurement features on the extracted surface. The main design intentions of the smart 3D tolerance tags are to provide a high-level overview of the evaluated tolerances, to give more details on demand, and to allow an easy navigation to the tolerance of interest for a further detailed evaluation.

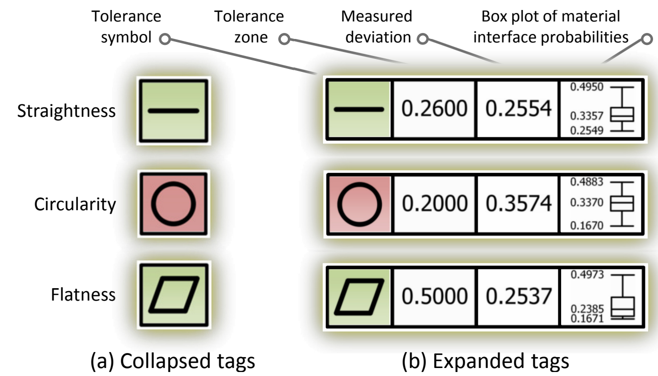

Figure 5: Smart 3D tolerance tags.

An example of smart 3D tolerance tags is given in Figure 4. Each 3D tolerance tag is represented as a rectangular billboard attached to a certain point in 3D (anchor) using a leader line. The anchor point is located at the center of the corresponding reference shape. Smart tags are rendered as an overlay on top of the 3D view. In this way tags are never occluded by the specimen's surface and can only be occluded by other tags.

The smart tolerance tags provide information about a measured tolerance at two levels-of-detail in two modes: the collapsed mode and the expanded mode. Individual tags can be collapsed or expanded by a right mouse click. To provide an overview of the performed measurements, the tags are usually shown in the collapsed mode (Figure 4). Collapsed tags allow for a quick identification of the tolerance type and checking if the corresponding tolerance is met. They only show symbols of the corresponding geometric tolerances (Figure 5). The background of the symbol is colored green if the measured deviation is within the allowed tolerance and red if the allowed tolerance is exceeded. If the user is interested in more details about a particular measurement feature, the smart tags can be expanded (Figure 5). Expanded tags additionally show the specified tolerance in the measurement plan, the measured tolerance itself, and a box plot encoding the distribution of the material interface probabilities of the probed points. They depict parameters such as: the biggest and the smallest interface probability, the upper and the lower quartiles, and the median value. The numeric values on the expanded 3D tags provide a quantitative overview of the tolerance data. If the user is interested in an even more detailed investigation of the measurement, the smart tag can be picked through user interaction. The picked tag will be highlighted with an orange halo and a corresponding measurement plot will be automatically displayed allowing a detailed visual exploration (Figure 2).

6 Reference Shapes

Every measurement has its corresponding reference shape defined in the measurement plan. We visualize reference shapes in the 3D view combined with the extracted surface as context (see Figure 4).

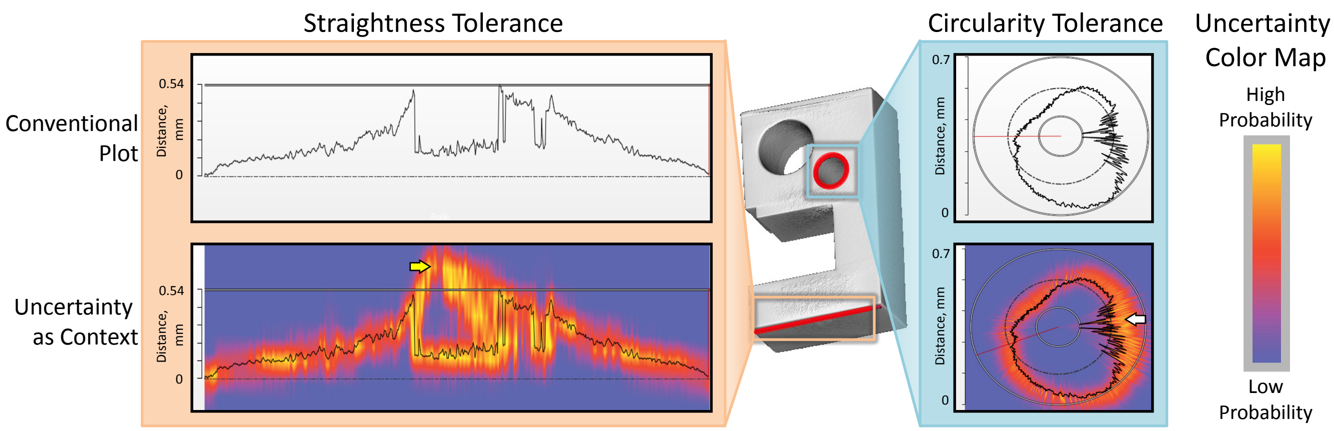

Figure 7: Visualizations of measurement plots. The color map used for the uncertainty as context visualizations is shown on the right. A duct tape artifact is marked with a yellow arrow. A noisy measurement area is pointed out with a white arrow.

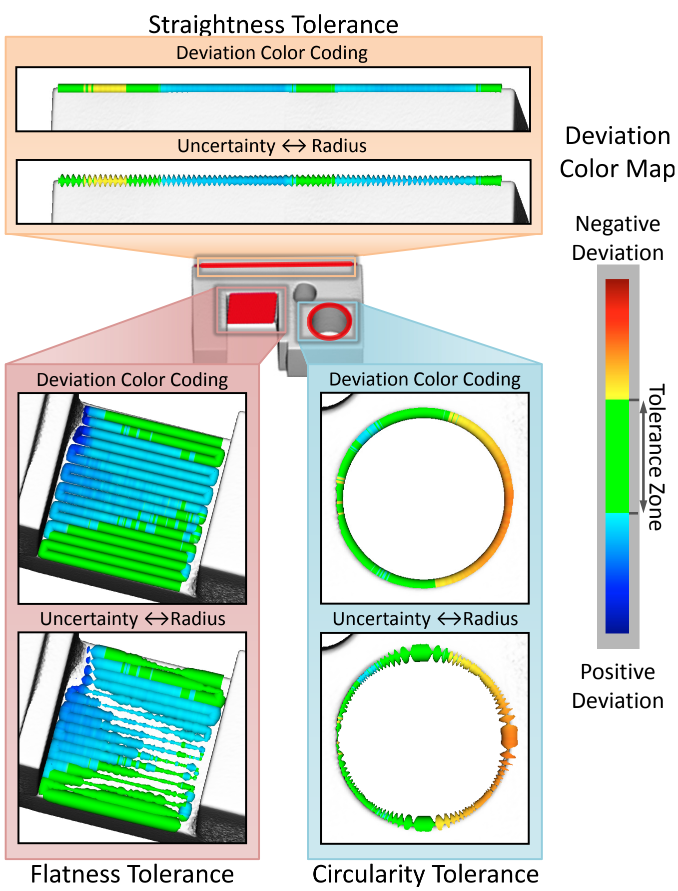

Figure 6: Reference shape visualizations. The deviation color map is shown on the right. Reference shapes are shown in red for a better visibility.

This allows the user to intuitively identify locations of measured features on the specimen surface and provides an additional visual clue about the type of the geometric tolerance. A line segment indicates the straightness tolerance, a circle indicates the circularity tolerance, and a space-filling line indicates the flatness tolerance. We are using tubular structures to represent the reference shapes. First, a poly-line is calculated for the reference primitive. Points of the poly-line correspond to positions where the probing is done. The poly-line is then used as a center-line for the corresponding tubular structure generation.

The default reference primitive is represented with a tubular structure (Figure 4 and 6). To provide the next level-of-detail we extend this visualization of the reference shapes. We map measurement parameters to the visual properties of the reference shapes. To provide an overview of the measurement parameters, we color code the deviation along a reference shape. An example of deviation color coding is given in Figure 6. Our goal is to quickly allow the user to detect measurement areas which are outside the tolerance zone and to estimate the direction and the value of deviations. For this purpose we apply a deviation color map commonly used for 3DXCT metrology applications (see Figure 6). This color map encodes deviation values within the tolerance zone in green. Strong positive deviations are colored in dark blue and strong negative deviations in dark red. This color scheme is familiar to the 3DXCT metrology specialists and permits quick visual analysis of the deviations. To provide an additional overview of the underlying measurement uncertainty, the measured points' interface probabilities can be mapped to the thickness of the tube (see Figure 6). The points with a low material interface probability are displayed with a large tube radius and the points with higher probability values are displayed with a small tube radius. This results in a blob-like appearance of areas with high uncertainty.

7 Measurement Plots

Figure 7 shows interactive measurement plots. They allow to navigate to the points of interest. The straightness plot supports scaling and panning interactions. The circularity plot supports scaling interactions. The visual linking of the measurement plot and the 3D view is implemented using a *sliding pointer* (Figure 2). The sliding pointer highlights a selected probed point in both the 3D view and the measurement plot. In the 3D view the pointer is represented as a red arrow indicating the selected point and aligned according to

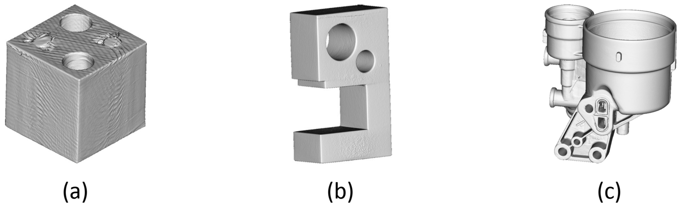

Figure 8: The CUBE (a), the TP09 (b), and the OFH (c) specimens.

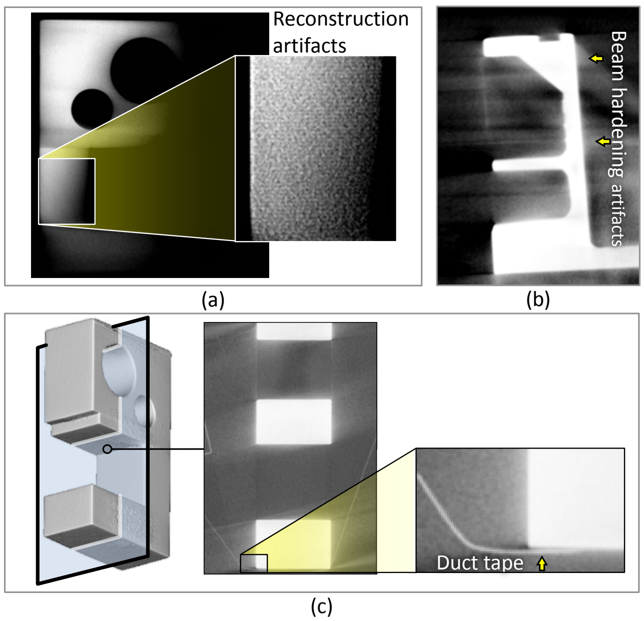

Figure 9: Various problems shown using slices through the original data.

the probing direction. In the measurement plot the selected point is highlighted with a red vertical line (Figure 2 left/bottom). The position of the pointer is updated when the user hovers a mouse over the measurement plot.

Showing the uncertainty distribution around the measurement profile in some cases can provide domain experts with a better notion on the reliability of the measurement. To achieve this we use the *uncertainty as context visualization*. Examples of the uncertainty as context visualization for the circular polar plot and the straightness plot are given in Figure 7. First, we calculate the uncertainty context image and then use it as the background image for the measurement plot. For every pixel of the profile plot canvas we find the corresponding position in the 3D volume and sample the interface probability at this position. We map uncertainties to colors using a heat color map (Figure 7 right). This technique provides domain experts with additional insight into the underlying uncertainty of the measurement. It enhances conventional measurement plot representations without introducing any conceptual changes. The uncertainty as context representation allows the user to visually estimate the uncertainty distribution around the measured points.

8 Results

For the evaluation of the presented methods we used two test specimens and one real world component. The first specimen *CUBE* (Figure 8a) is a component consisting of two materials: metal and plastic. It is a plastic cube with four drill holes: two larger ones and two smaller ones with steel pin insertions. The data of this test part were obtained using a simulation tool for 3DXCT scans by Reiter et al. [Reiter et al. 2011]. The reconstructed 3D volume has a resolution of $256\times256\times256$ voxels. Specimen two *TP09* (Figure 8b) is an aluminium test part used for evaluating beam hardening artifacts. The dataset for TP09 was obtained by a real 3DXCT scan with a resolution of $984\times984\times884$ voxels. The last specimen is an oil filter housing (*OFH*) (Figure 8c), i.e., a real-world industrial component with complex geometry. It has a dataset size of $529\times771\times873$ voxels. For the mentioned specimens we study a set of measurement features using the presented visualization techniques. In the following paragraphs we discuss the usefulness of our method and describe potential use cases.

Reconstruction artifacts in the form of high frequency stripes (Figure 9a) are present in all datasets. These artefacts are the result of periodic intensity fluctuations on the surface of the specimen. Due to their very high frequencies and local presence only at the surface, reconstruction artifacts are hardly visible in the data and require careful window function adjustments to visually reveal their presence. A depiction of reconstruction artifacts for the straightness tolerance is shown in Figure 10. Periodic patterns in the uncertainty as context visualization indicate the presence of reconstruction artifacts. In this case, the visualization provides the user with additional insight into the data, which is not possible with default exploration techniques such as measurement plots and slice views.

Low contrast in the intensity values at the surface of the specimen appear in parts of the reconstructed volume due to 3DXCT artifacts like beam hardening. Artifacts-affected areas appear as *noisy regions* on the extracted isosurface. The noise will also appear in the profile line, hindering the evaluation of actual deviations. An example of such an area for the circularity tolerance is shown in Figure 7 on the right side of the polar plot. In this case the uncertainty as context visualization provides the user with information about where the actual surface of the noisy part is likely to be. In this example it can be seen that noise creates some outliers towards the center of the reference circle. The actual surface is with higher probability located on the outer side of the profile line.

In some cases conventional measurement plots fail to provide the user with insight about the source of deviations. They only show the profile line and do not provide any *context information about surroundings* of the profile. In Figure 7 the yellow arrow in the straightness plot indicates that there are some abnormal variations in the middle section of the profile. These variations are actually caused by a duct tape which was used by the technicians to fix the specimen on the rotary plate of the 3DXCT device (Figure 9c). In the middle of the measurement feature the duct tape closely approaches the actual surface of the specimen. This causes the extracted isosurface to change between the surface of the specimen and the surface of the duct tape. It can be seen that this situation is reflected in the measurement plot with uncertainty as context visualization. In the uncertainty as context visualization the probability interface forms two high probability zones. The profile line significantly varies by jumping from one probability zone to the other one. The provided visualization enables metrology experts to quickly identify the source of such abnormal behaviour and to draw proper conclusions (e.g., changing the duct tape placement).

Additionally, excluding inhomogeneities caused by artifacts from the measurement result helps to provide more accurate metrology results. The slice image illustrating beam-hardening artifacts in Figure 9b shows intensity inhomogeneities along the measurement. A straightness measurement performed on an area affected by beam-hardening artifacts for the OFH specimen is shown in Fig-

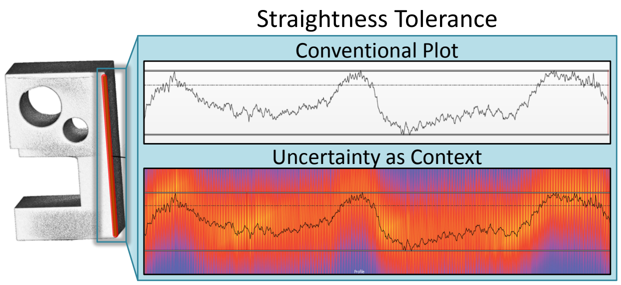

Figure 10: Depiction of reconstruction artifacts through different visualizations.

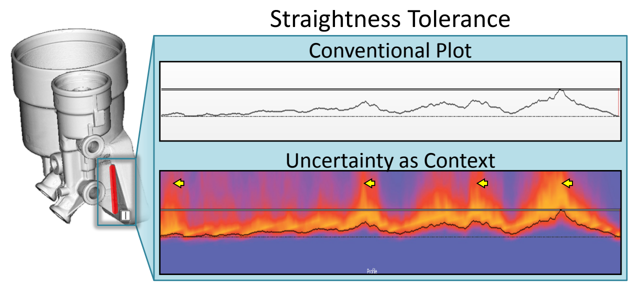

Figure 11: Depiction of beam-hardening artifacts through different visualizations.

ure 11. The conventional measurement plot is not providing any information about *the reliability of different parts* of the measurement. In contrast, uncertainty as context visualization clearly depicts uncertain areas in the surrounding interface probabilities (yellow areas). In case these areas have high deviation values, the knowledge about their reliability can strongly affect the judgement of CT metrologists.

We collected *domain experts feedback* on the presented methods from our industrial metrology company partners to evaluate the practical value of the proposed visualization techniques. Three experts from the company partner dealing with industrial 3DXCT metrology on a daily basis and for extended periods of time have participated. Furthermore, three experts from a CT research group have participated. Two of them are dealing with industrial 3DXCT metrology on a weekly basis and also have extended work experiences in the field. The evaluation has assessed the presented visualizations including smart 3D tolerance tags, reference shapes, and measurement plots as well as interactivity of the measurement plots, and visual linking of views. The results of the evaluation questionnaire are presented in Table 1. In this table, '++' indicates a highly positive judgement, '+' indicates a positive judgement, and '+/-' indicates predominantly positive judgement. The participants appreciated the idea of visualizing measurement information on the reference shapes and considered the deviation color coding on the reference shapes to be from helpful to very helpful. The interactivity of the measurement plots was considered helpful by most participants with the scaling functionality of the circularity plot considered as especially important for the domain specialists. All participants except one have felt that the idea of smart 3D tolerance tags for providing an overview of measurements is very helpful. Two of three company experts have valued the visual linking employing the sliding pointer to be highly useful. Several experts have indicated that uncertainty visualizations for the measurement plots are only useful in certain cases. For low-resolution data, uncertainty representations were rated as unhelpful. One expert pointed out that uncertainty information is not useful in several cases due to the influence of reconstruction artifacts.

Smart 3D tolerance tags	displaying in 3D	++
	box plots	+
Reference shapes	tubular lines	+/-
	deviation color coding	++
	uncertainty to radius	++
Measurement plots	uncertainty as context	+/-
	interactivity	+
Visual linking of views	sliding pointer	+
	linking via picking	+

Table 1: Summary of the evaluation questionnaire.

9 Conclusions

We have presented a metrology workflow for industrial specimens which is reflecting the fuzziness of common geometric tolerancing using 3DXCT. The presented approach determines the material interface probabilities. Applying a statistical analysis approach on the reconstructed 3D volume data in order to estimate the probabilities of material interface locations. The obtained uncertainty information is then incorporated in a set of novel visualization methods at various levels-of-detail. The proposed visualizations are: smart 3D tolerance tags, reference shapes supporting deviation color coding, as well as mapping uncertainty to radius, and measurement plots utilizing uncertainty as context. The views containing the visualizations are linked using sliding pointers and 3D tolerance tag picking. These visualizations provide the user with insight into measurement fuzziness and reliability while preserving the usual metrology workflow. The presented integrated visualizations provide information about the uncertainty of measurements on various levels-of-detail. Our system is implemented as an integrated tool performing data preprocessing and utilizing linked interactive views to support the exploration and visualization of the measurements' uncertainty. We test the presented methods using various specimens like simulated low-resolution datasets and high-resolution scanned datasets.

In this work we assume that probability distributions obtained from the Bayesian classification are independent. This approximation can lead to an overestimation of the interface probabilities. Incorporating the estimation of correlations in the data is a promising topic for further research. In future work we want to include more types of geometric tolerances in our system. More complex geometric tolerances might require additional adjustments of the visualization techniques. Furthermore 3D visualizations can be beneficial for such tolerances as 2D representations and measurement plots might not be sufficiently intuitive. In addition, there is a wide field for exploring various new 3D visualization techniques that reflect the fuzziness of tolerances such as flatness or cylindricity. Despite the mentioned limitations, the presented system shows promising results in providing metrology experts with insight into the uncertainty of the measurements which was not considered before. Taking this new information into account can help in improving 3DXCT geometric metrology and tolerancing and in achieving a more reliable quality control.

Acknowledgements

This work is supported by the K-Project for non-destructive testing and tomography (http://www.3dct.at) of the Austrian Research Promotion Agency (FFG) grant number 820492. We would also like to thank domain experts from Carl Zeiss for their valuable feedback and answering the questionnaire.

References

AMIRKHANOV, A., HEINZL, C., REITER, M., AND GRÖLLER, M. E. 2010. Visual Optimality and Stability Analysis of 3DCT Scan Positions. *IEEE Transactions on Visualization and Computer Graphics* (10), 1477 – 1487.

BALL, J., AND MOORE, A. 1997. *Essential Physics for Radiographers. 3rd ed.* Blackwell Science, Oxford.

BERGER, W., PIRINGER, H., FILZMOSER, P., AND GRÖLLER, E. 2011. Uncertainty-Aware Exploration of Continuous Parameter Spaces Using Multivariate Prediction. *Computer Graphics Forum 30*, 3 (6), 911 – 920.

CONINX, A., BONNEAU, G., DROULEZ, J., AND THIBAULT, G. 2011. Visualization of Uncertain Scalar Data Fields Using Color Scales and Perceptually Adapted Noise. *Applied Perception in Graphics and Visualization*.

DJURCILOV, S., KIM, K., LERMUSIAUX, P., AND PANG, A. 2002. Visualizing Scalar Volumetric Data With Uncertainty. *Computers & Graphics 26*, 2 (04), 239 – 248.

GRIGORYAN, G., AND RHEINGANS, P. 2004. Point-Based Probabilistic Surfaces to Show Surface Uncertainty. *IEEE Transactions on Visualization and Computer Graphics 10*, 5, 564 – 573.

HEINZL, C., KASTNER, J., MÖLLER, T., AND GRÖLLER, E. 2008. Statistical Analysis of Multi-Material Components Using Dual Energy. *In Proceedings of the 13th International Fall Workshop Vision, Modeling, and Visualization*, 179 – 188.

HEINZL, C. 2009. *Analysis and Visualization of Industrial CT Data*. PhD thesis, Institute of Computer Graphics and Algorithms, Vienna University of Technology.

HENZOLD, G. 2006. *Geometrical Dimensioning and Tolerancing for Design, Manufacturing and Inspection: a Handbook for Geometrical Product Specifications Using ISO and ASME Standards*. Butterworth-Heinemann.

JOHNSON, C. 2004. Top Scientific Visualization Research Problems. *Computer Graphics and Applications, IEEE 24*, 4 (7 – 8), 13 – 17.

KASPERL, S., BAUSCHER, I., HASSLER, U., MARKERT, H., AND SCHRÖPFER, S. 2002. Reducing Artifacts in Industrial 3D Computed Tomography (CT). In *VMV*, 51 – 57.

KNISS, J., VAN UITERT, R., STEPHENS, A., LI, G., TASDIZEN, T., AND HANSEN, C. 2005. Statistically Quantitative Volume Visualization. *IEEE Visualization 2005 6*, 37 – 37.

KRUTH, J., VANHERCK, P., AND VAN DEN BERGH, C. 2001. Compensation of Static and Transient Thermal Errors on CMMs. *Annals of the CIRP, Paris 50*, 1, 377 – 380.

KRUTH, J. P., BARTSCHER, M., CARMIGNATO, S., SCHMITT, R., DE CHIFFRE, L., AND WECKENMANN, A. 2011. Computed Tomography for Dimensional Metrology. *CIRP Annals Manufacturing Technology 60*, 2, 821 – 842.

LUNDSTRÖM, C., LJUNG, P., AND YNNERMAN, A. 2006. Local Histograms for Design of Transfer Functions in Direct Volume Rendering. *IEEE Transactions on Visualization and Computer Graphics 12*, 6, 1570 – 9.

LUNDSTRÖM, C., LJUNG, P., PERSSON, A., AND YNNERMAN, A. 2007. Uncertainty Visualization in Medical Volume Rendering Using Probabilistic Animation. *IEEE Transactions on Visualization and Computer Graphics 13*, 6, 1648 – 55.

PAULY, M., MITRA, N., AND GUIBAS, L. 2004. Uncertainty and Variability in Point Cloud Surface Data. In *Eurographics symposium on point-based graphics*, Citeseer, vol. 84.

PFAFFELMOSER, T., REITINGER, M., AND WESTERMANN, R. 2011. Visualizing the Positional and Geometrical Variability of Isosurfaces in Uncertain Scalar Fields. *Computer Graphics Forum 30*, 3 (6), 951 – 960.

PÖTHKOW, K., AND HEGE, H.-C. 2010. Positional Uncertainty of Isocontours: Condition Analysis and Probabilistic Measures. *IEEE Transactions on Visualization and Computer Graphics* (10), 1 – 15.

PÖTHKOW, K., WEBER, B., AND HEGE, H.-C. 2011. Probabilistic Marching Cubes. *Computer Graphics Forum 30*, 3 (6), 931 – 940.

PRASSNI, J.-S., ROPINSKI, T., AND HINRICHS, K. 2010. Uncertainty-Aware Guided Volume Segmentation. *IEEE Transactions on Visualization and Computer Graphics 16*, 6, 1358 – 65.

REITER, M., HARRER, B., SALABERGER, D., HEINZL, C., GUSENBAUER, C., KUHN, C., AND KASTNER, J. 2011. Simulation Aided Study for Optimising Device Parameters of an Industrial X-Ray Computed Tomography System for Non-Destructive Testing and Materials Characterisation. *International Symposium on Digital Industrial Radiology and Computed Tomography 2011, Berlin/GE* (6).

RHEINGANS, P., AND JOSHI, S. 1999. Visualization of Molecules With Positional Uncertainty. In *Data Visualization '99, Proceedings of the Joint EUROGRAPHICS - IEEE TCVG Symposium on Visualization*, Springer-Verlag, vol. 99, 299 – 306.

RHODES, P., LARAMEE, R., BERGERON, R., AND SPARR, T. 2003. Uncertainty Visualization Methods in Isosurface Rendering. In *Eurographics*, Citeseer, 83 – 88.

SAAD, A., HAMARNEH, G., AND MÖLLER, T. 2010. Exploration and Visualization of Segmentation Uncertainty Using Shape and Appearance Prior Information. *IEEE Transactions on Visualization and Computer Graphics 16*, 6, 1366 – 75.

SHNEIDERMAN, B. 1996. The Eyes Have It: A Task by Data Type Taxonomy for Information Visualizations. In *Proceedings of the 1996 IEEE Symposium on Visual Languages*, IEEE Computer Society, 336 – 343.

WASER, J., RIBIČIĆ, H., FUCHS, R., HIRSCH, C., SCHINDLER, B., BLÖSCHL, G., AND GRÖLLER, E. 2011. Nodes on Ropes: A Comprehensive Data and Control Flow for Steering Ensemble Simulations. *IEEE Transactions on Visualization and Computer Graphics 17*, 12 (11), 1872–1881.

ZUK, T., AND CARPENDALE, S. 2006. Theoretical Analysis of Uncertainty Visualizations. In *Proceedings of SPIE*, Citeseer, vol. 6060, 66 – 79.